


METHODOLOGY

Open Access



Forward modelling and identification of shallow gas in the Bohai Bay seabed

Xiao-Di Yang^{1,2*} , Ming-Hao Chun^{1,2}, Xiao-Qiao Luo^{1,2} and Zhi-Guang Yao^{1,2}

Abstract

The accumulation of shallow gas in the seabed reduces the strength of strata or forms a high-pressure air sac, endangering ocean engineering construction. Therefore, it is important to identify the distribution of shallow gas in the seabed within the study area. Shallow gas increases the soil mass porosity and reduces the acoustic wave velocity, causing attenuation by absorbing to high-frequency components in the acoustic waves. Based on the geological drilling data in the area surrounding an oil platform in Bohai Bay, a stratigraphic model was established for forward analysis, and the results suggest the presence of the phase inversion of reflective waves at the interface between shallow gas and strata and sunken events for the lower shallow gas. According to a survey of stratigraphic profiles surrounding the platform, a seismic attribute analysis of acoustic stratigraphic profile data concerning amplitude, instantaneous phase, and instantaneous frequency was carried out, and characteristics such as disordered weak amplitude reflection, phase inversion, sunken events and indicators, including high-frequency loss and shallow gas reflection, were identified. Given that the shallow gas reflection is columnar and ended at the top clay strata of the seabed, the shallow gas was probably produced from deep depths.

Keywords: Seabed shallow gas, Forward analysis, Instantaneous phase, Instantaneous frequency, Identification of shallow gas

Introduction

Shallow gas refers to gas that accumulates at a depth of 1000 m beneath the seabed. Shallow gas is characterized by small molecules, low density, weak absorbability and strong diffusivity. It is easily accumulates and transfers in strata. When shallow gas accumulates in strata, it changes the physical mechanical properties of strata, resulting in increased porosity, reduced compactness, and poorer strength of the strata (Whelan et al. 1977; Li et al. 2013; Wang et al. 2011, 2021; Shang et al. 2013; Sun and Huang 2014). In the case of an external load, the gas-containing stratum may incur creepage, causing subsidence or sliding of the foundation. Furthermore, in the case of shallow gas with a well overlying the cap,

a specific air pressure sac is present. When the overlying strata are punctured during ocean engineering, such as oil platform construction and drilling, the shallow gas surges out due to internal pressure and causes blowout accidents. Therefore, identifying the distribution characteristics of shallow gas within work areas is of great significance to the selection and evaluation of construction sites in ocean engineering.

There are two types of shallow gas in the seabed: the first is biomethane, whose main composition is methane. Due to decomposition by methane bacteria, biomethane is gradually formed from biodebris and organic substances in the strata. Biomethane mainly exists in the shallow strata. The second is thermogenic methane, which exists in a high-temperature and high-pressure environment at a depth of 2000 m beneath the seabed. It consists of hydrocarbons formed from kerogen cracking and often develops a hyperpressure air sac; sometimes, it also rises and

*Correspondence: yangxiaodi1989@126.com

¹ CNPC Research Institute of Engineering Technology, JinTang Road 40#, Binhai New District, Tianjin, China

Full list of author information is available at the end of the article

transfers through the pores, cracks and broken profiles of rocks to accumulate in the shallow strata.

Currently, acoustic detection is generally adopted for the identification of shallow gas, where it is based on the characteristics of acoustic stratigraphic profiles, such as acoustic blankets, acoustic disturbances, acoustic curtains, irregular strong reflections at top interfaces, sunken phases on both sides and sunken events caused by decreases in acoustic wave velocity (Woodside et al. 2003; Yan et al. 2007; Gu et al. 2008, 2009b; Wang et al. 2014; Yang et al. 2020, 2015). These amplitude characteristics of the acoustic wave are mainly utilized in this method. However, as these characteristics are sufficient conditions for the identification of shallow gas, there might be multiple solutions. Therefore, multiple seismic attributes are used in this study for the identification of shallow gas to improve the accuracy in the identification of shallow gas. The research process is shown in Fig. 1.

Acoustic wave detection technology

At present, acoustic detection technology is the main technology for the detection of shallow gas. For shallow gas with different causes of formation, their accumulation state and acoustic wave reflection characteristics in strata also vary. Acoustic waves are a form of energy transfer. In media with different strengths, structures and densities, the transmission velocity, frequency components, energy decrement and other wave field characteristics of acoustic waves also change (Lei et al. 2007).

The transmission equation of acoustic waves in water and strata is:

$$\begin{cases} \rho \frac{\partial^2 u}{\partial t^2} = \frac{\partial \sigma_{xx}}{\partial x} + \frac{\partial \sigma_{xy}}{\partial y} + \frac{\partial \sigma_{xz}}{\partial z} + \rho F_x \\ \rho \frac{\partial^2 v}{\partial t^2} = \frac{\partial \sigma_{xy}}{\partial x} + \frac{\partial \sigma_{yy}}{\partial y} + \frac{\partial \sigma_{zy}}{\partial z} + \rho F_y \\ \rho \frac{\partial^2 w}{\partial t^2} = \frac{\partial \sigma_{xz}}{\partial x} + \frac{\partial \sigma_{yz}}{\partial y} + \frac{\partial \sigma_{zz}}{\partial z} + \rho F_z \end{cases}, \quad (1)$$

where t is time; ρ is the density of the medium; $u, v, \text{ and } w$ are displacements in the $x, y, \text{ and } z$ directions; $\sigma_{xx}, \sigma_{xy}, \sigma_{xz}, \sigma_{yy}, \sigma_{yz}, \text{ and } \sigma_{zz}$ are stresses; and $F_x, F_y, \text{ and } F_z$ are the stresses in the external force in the $x, y, \text{ and } z$ directions.

The three-dimensional equation of even isotropous ideal elastic media expressed in vector form is:

$$\rho \frac{\partial^2 \mathbf{S}}{\partial t^2} = (\kappa + \mu) \text{grad} \theta + \mu \nabla^2 \mathbf{S} + \rho \mathbf{F}, \quad (2)$$

where $\mathbf{F} = F_x \mathbf{i} + F_y \mathbf{j} + F_z \mathbf{k}$ is the vector of the external force; $\mathbf{S} = u \mathbf{i} + v \mathbf{j} + w \mathbf{k}$ is the vector of the displacement; $\text{grad} \theta = \frac{\partial \theta}{\partial x} \mathbf{i} + \frac{\partial \theta}{\partial y} \mathbf{j} + \frac{\partial \theta}{\partial z} \mathbf{k}$ is the vector of the gradient; ∇^2 is the Laplace operator; ρ is the density of the medium; κ and μ are Lamé constants; and t is time. Equation (2) is rewritten into a plane harmonic equation:

$$p(x_i, t) = p_0 \sin \left(\frac{2\pi x_i}{\lambda} - \omega t + \phi \right), \quad (3)$$

where t is time; p is the acoustic wave signal in the time domain; p_0 is the acoustic wave amplitude; λ is wavelength; $\omega = 2\pi f$ is the angular frequency; and ϕ is the phase shift. In acoustic stratigraphic detection, the acoustic wave created by an energy converter can be deemed the superposition of multiple simple harmonic waves.

Seismic attributes

Seismic attributes are properties for the description and quantification of seismic data, and they are a subset of all information included in raw seismic data. The acquisition of seismic attributes is a process of decomposing seismic data, where each seismic attribute is a subset of seismic data. In view of the applied geophysics, seismic attributes are seismic characteristics for depicting and describing geological information, such as the stratigraphic structure, lithology and physical properties.

Amplitude

Amplitude is the most frequently used seismic attribute. The amplitude of acoustic wave reflection is the convolution of the acoustic wave and the strata's reflective coefficient, reflecting the changes in the strata's nature. The change in acoustic waves caused by strata is referred to as wave impedance, which is the product of the media's density ρ and acoustic wave velocity v . When acoustic waves penetrate into the interface of different neighbouring media, reflection and transmission occur. The reflective coefficient of strata is:

$$R = \frac{\rho_2 v_2 - \rho_1 v_1}{\rho_2 v_2 + \rho_1 v_1}, \quad (4)$$

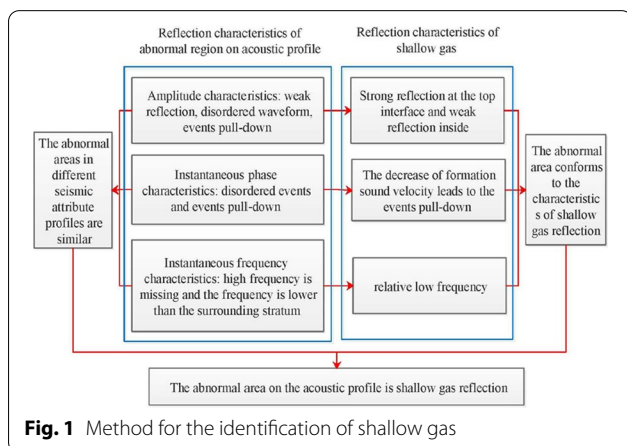


Fig. 1 Method for the identification of shallow gas

where ρ_1, v_1, ρ_2 and v_2 are the density and acoustic wave velocity of media above and below the interface, respectively. Strata with different natures often have different densities and acoustic wave velocities. At their interface, the reflective coefficient is not zero. Furthermore, the greater the difference between strata is, the greater the absolute value of the reflective coefficient at the interface and the greater the amplitude of the reflective wave.

Instantaneous phase

Based on the change in phases when acoustic waves penetrate different geologic bodies, the boundary of geologic bodies may be identified. The instantaneous phase is the resolution of signals:

$$Ph(t) = \frac{180}{\pi} \arctan \left[\frac{g(t)}{f(t)} \right], \tag{5}$$

where t is time and $g(t)$ and $f(t)$ are the real and virtual parts of the signal, respectively.

The phase information is irrelevant to the amplitude but relates to the transmission phase of the acoustic wave wavefront. It is a physical property of acoustic waves and is not affected by the waveform or amplitude. Furthermore, it accurately demonstrates the reflection area of weak amplitude and can be used for the identification of the continuity and boundaries of strata (Mou et al. 2007).

Instantaneous frequency

The instantaneous frequency is the time derivative of the instantaneous phase, which is related to the frequency spectrum of the acoustic wave. The instantaneous frequency $\phi(t)$ (Hz) is the rate of change of the phase over time:

$$\phi(t) = \frac{d[Ph(t)]}{dt}, \tag{6}$$

where t is time; $\phi(t)$ is the instantaneous frequency; and $Ph(t)$ is the instantaneous phase.

The instantaneous frequency is related to the nature of the strata that the acoustic wave passes through. The instantaneous frequency is a physical property of acoustic wave signals related to the density of strata. Generally, it may serve as an indicator of the oil and gas zone, fracture zone and thickness of strata. When there is oil or gas in strata, the high-frequency components often incur attenuation by absorption (Sager et al. 1999; Orange et al. 2005; Hou et al. 2013; Hu 2010).

Forward modelling of shallow gas

During transmission in strata, the attenuation of acoustic wave energy may be divided into two parts: nonintrinsic attenuation and intrinsic attenuation. Nonintrinsic

attenuation is mainly caused by the geometric diffusion of acoustic waves and the geometric structure of media; intrinsic attenuation is related to the viscoelasticity of rocks, which converts the vibration energy of acoustic waves into thermal energy. In porous media filled with fluid, intrinsic attenuation is dominant. In porous media, the relative movement between solids and fluids (gas or water) is the main cause of the energy attenuation of acoustic waves (Li 2015).

The porosity of the strata increases when shallow gas accumulates, thus influencing the density and acoustic wave velocity in the strata. For the strata, the increased porosity causes reduced density. However, the acoustic wave velocity in strata is related to the porosity and water content, where the following empirical formula is available (Zou et al. 2007, 2008; Long and Li 2015):

$$v = 1981.7539 \times (0.9958 - 0.004n + 0.0002\omega) \tag{7}$$

where v is the velocity of the acoustic wave, n is the porosity (%) of the strata, and ω is the water content (%).

Biomethane often exists in shallow layers in the form of isolated air sacs or acoustic blankets, with little vertical continuity; thermogenic methane often moves from bottom up in the form of columns, with profound vertical continuity. Based on the causes of the formation of shallow gas and its ascertained forms, it is assumed that biomethane is in the form of an isolated air sac, while thermogenic methane is in the form of vertical columns. To study the acoustic reflection characteristics of shallow gas with 120 m-depth geological drilling data from Bohai Bay, a forward model of normal strata, a model of strata with shallow gas air sacs and a model of strata with column-shaped shallow gas were established. The drilling data are as Table 1.

Based on the characteristics of strata, such as the acoustic wave velocity and wave resistance, the strata are divided into six layers whose distribution is as Table2. The acoustic wave velocity and density of each layer are calculated via the weighted average.

A two-dimensional stratigraphic model was built using the data in Table 2, where the width was 2000 m and the depth was 120 m, with a mesh of 2 m × 2 m. According to a survey in the Hangzhou subway project (Guo et al. 2010), the strata contain shallow gas. Shallow gas mostly exists in sandy clay, while muddy clay is the overlying cap. The shallow gas has a maximum pressure of 0.405 MPa; the strata containing shallow gas have a water content of 7%, a saturation of 20%, a density of 1.49 g/cm³, a porosity of 49% and an acoustic wave velocity of 1588 m/s.

The forward model adopted the acoustic wave equation, with an offset of zero. The Ricker wavelet was used as the excitation wavelet, with a main frequency of 250 Hz, a phase of zero and a frequency bandwidth

Table 1 Geological drilling data sheet

No	Depth of bottom layer/m	Sediment type	Water content %	Wet bulk density N/cm ³	Proportion	Porosity %	Acoustic wave velocity m/s
1	2.4	Soft clay	55	16.5	2.7	62	1506
2	3.3	Medium dense silt	21	20.4	2.71	39	1671
3	14.5	Muddy clay	38	18.5	2.72	51	1588
4	16.7	Silty fine sand	26	19.3	2.69	45	1627
5	19.8	Hard silt	26	19.7	2.7	43	1643
6	22	Dense silt	23	20	2.72	42	1651
7	25.7	Dense silty fine sand	20	20.5	2.68	38	1684
8	28.8	Dense silt	28	19.1	2.68	46	1621
9	34.8	Hard clay	37	18.5	2.69	50	1594
10	40.6	Dense silt	23	19.6	2.71	44	1635
11	49.8	Silty clay	27	20.4	2.71	39	1674
12	55.7	Dense silt	26	19.6	2.7	44	1638
13	58.8	Hard clay	35	18.2	2.71	52	1575
14	61.7	Dense fine sand	24	19.2	2.7	46	1619
15	81.1	Hard silty clay	30	19.8	2.72	43	1644
16	91.7	Dense sandy silt	21	19.9	2.72	42	1645
17	106.6	Hard silty clay	20	20.5	2.72	39	1673
18	111.1	Dense silt	26	19.5	2.71	44	1631
19	120.3	Hard silty clay	21	20.5	2.71	39	1676

Table 2 Stratum division sheet

Strata	Representative stratum	Depth of bottom layer /m	Formation thickness/m	Acoustic wave velocity m/s	Density g/cm ³
Layer-1	Soft clay	14.5	14.5	1573	1.81
Layer-2	Silty fine sand	25.7	11.2	1655	1.99
Layer-3	Hard clay	34.8	9.1	1603	1.87
Layer-4	Silt	49.8	15.0	1658	2.01
Layer-5	Dense silt	58.8	9.0	1616	1.91
Layer-6	Hard silty clay	120	61.2	1661	2.01

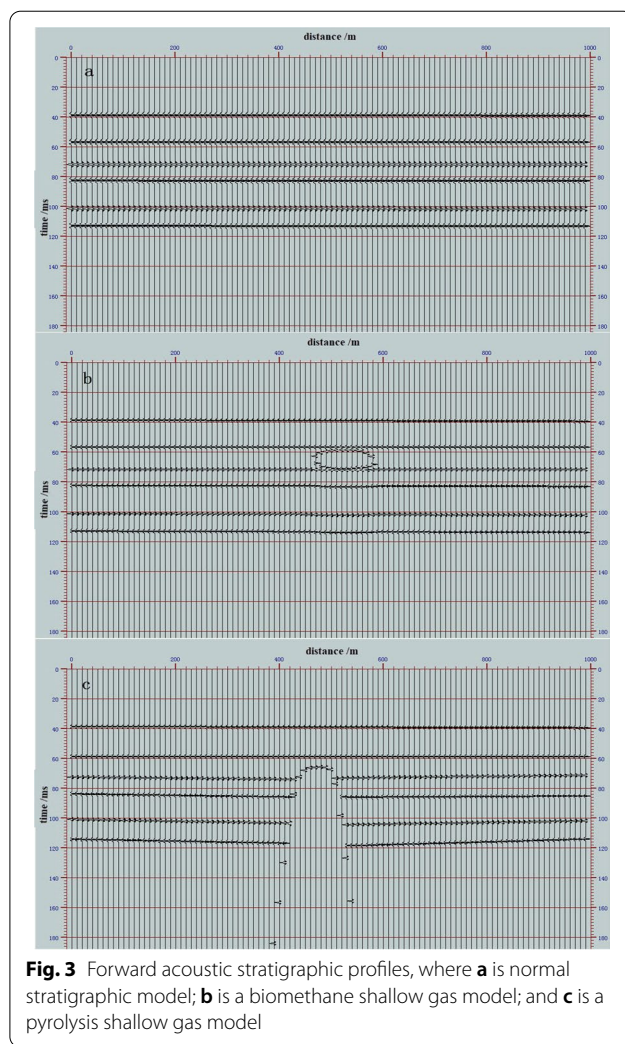
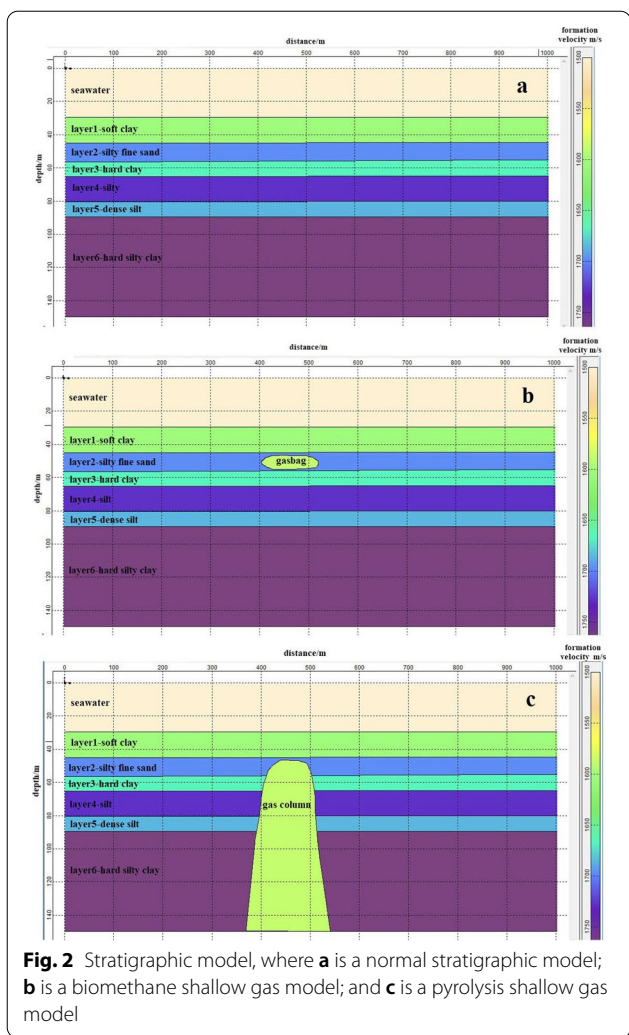
of 120 Hz. The continuation length of the wavelet was 10 ms. The constructed stratigraphic model is shown in Fig. 2 as follows. Biomethane is designed to exist in layer 2 (silty fine sand) in the form of an air sac (Fig. 2b). Thermogenic methane transfers upwards to shallow strata from deep strata and exists in layers 2, 3, 4, 5 and 6 in the form of columns (Fig. 2c).

The forward acoustic stratigraphic profile is shown in Fig. 3. Figure 3a shows that there were six continuous events that matched the interfaces between seawater and the five strata interfaces. The phase of the reflective wave events was negative at the interface between layer 2 and layer 3 and at the interface between layer 4 and layer 5, indicating that the reflective coefficient of the strata was negative. Based on the stratigraphic model, velocity reversions were present in layers 3 and 5, namely, the acoustic wave velocity in the lower strata was smaller

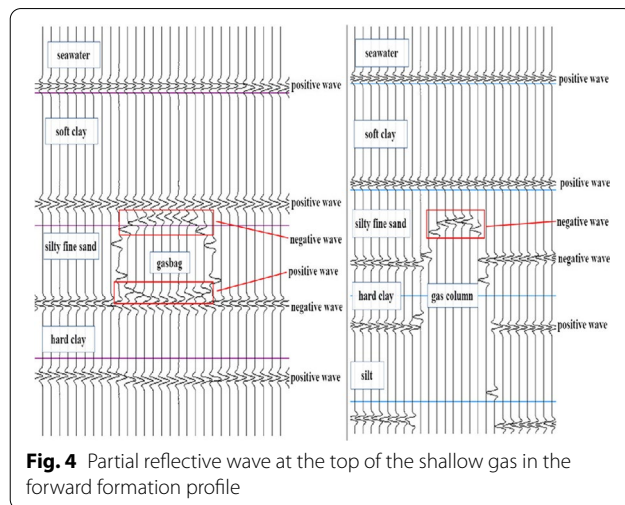
than that in the upper strata. In Fig. 3b, since a shallow gas air sac was present in layer 2 and the acoustic wave velocity in shallow gas was smaller than that in layer 2, the reflective wave phase at the top interface of the shallow gas was negative, while that at the bottom interface was positive. When the duration of the acoustic wave's travel time in shallow gas is greater than that in the strata, the reflective wave events in the lower shallow gas are sunken downwards. In Fig. 3c, since penetrating shallow gas occurred in the column-shaped strata beneath layer 2, the reflective wave phase at the top interface of the shallow gas was negative, while the reflection at the side interface was not clear.

The reflective wave at the top of the shallow gas in the forward formation profile is shown in Fig. 4.

When shallow gas is present in the strata, the physical properties and acoustic reflection characteristics of the



strata change. In normal strata, the internal nature of the same stratum is often relatively uniform with close wave resistance and a nearly zero reflective coefficient. When the strata contain shallow gas, the density and acoustic wave velocity of strata are reduced, as is the wave resistance; their reflective coefficient at the interfaces between strata and shallow gas are negative, forming a strong reflective interface and causing a specific shielding effect of the lower strata. When acoustic waves pass through strata that contain shallow gas, the attenuation of high-frequency components is increased, the acoustic wave velocity is reduced, and the travel time duration is increased. Seismic attribute analysis reveals that the characteristics of shallow gas reflective waves in the acoustic stratigraphic profile are as follows: ① the top interface is a strong reflection with phase reversion, while the lower interface is a weak reflection; ② the reduced acoustic wave velocity results in downwards sunken events; and ③ a relatively low frequency is demonstrated.



Analysis of measured seismic materials

In the Huanghua Sea of Bohai Bay, there are many shallow gas layers in the strata. Acoustic stratigraphic profile measurements were carried out for the area surrounding an oil platform. An electric spark was used with an excitation energy of 1000 J and a recording duration of 400 ms. Constellation difference GPS was adopted for navigation and positioning; the acoustic wave velocity in strata was 1550 m/s from the material surrounding the area. There was a suspected shallow gas reflection in the acoustic stratigraphic profiles. Since the gas-containing strata are selective in absorbing acoustic wave energy with different frequencies, the three seismic attributes of amplitude, instantaneous phase and instantaneous frequency were analysed for the acoustic stratigraphic profiles, and shallow gas was identified with multiple attributes. The survey area was a 1 km × 1 km square, and a grid survey line was adopted (Fig. 5). The coordinates of the centre of the survey area were 38°28'20.1094"N and 117°44'13.9174"E. Two profiles were selected for the analysis of seismic attributes: profile 1 and profile 2, and profile 1 matches Figs. 6, 8, 10 below; profile 2 matches Figs. 7, 9, 11 below.

Amplitude characteristics

On the amplitude profile, the reflection characteristics are shown in Figs. 6 and 7. Figure 6 shows that there was a weak reflection area bounded by green lines in the profile, which is likely the reflection of shallow gas. In this area, the energy of the reflection wave was weak, with non-contiguous events, unstable waveforms, disordered reflection and an insignificant layer structure; furthermore, there was apparent interruption with the

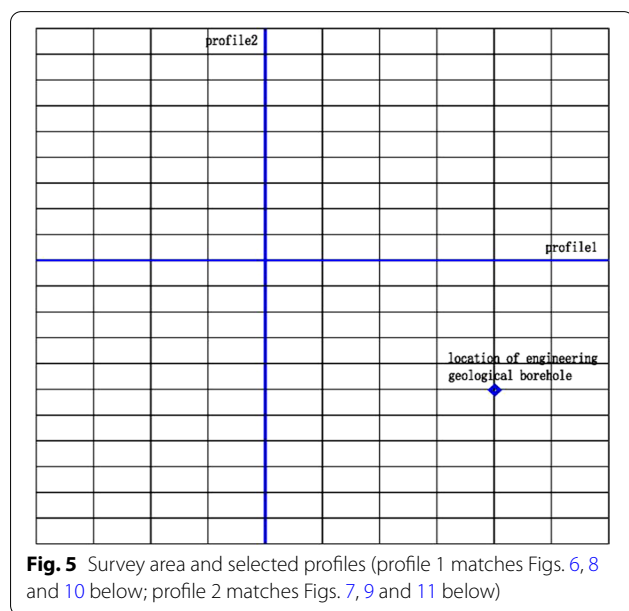


Fig. 5 Survey area and selected profiles (profile 1 matches Figs. 6, 8 and 10 below; profile 2 matches Figs. 7, 9 and 11 below)

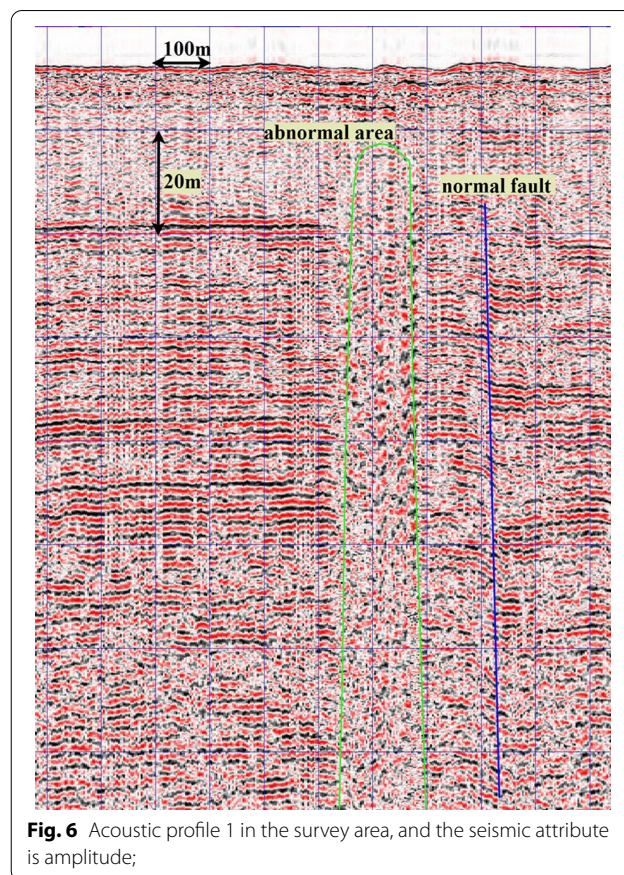


Fig. 6 Acoustic profile 1 in the survey area, and the seismic attribute is amplitude;

surrounding events, with apparent rougher and downwards bent events at the edge; the area extended upwards in the form of a column, with a width of approximately 110 m and a distance of approximately 15 m from the top to the seabed.

Figure 7 shows that there was a downwards sunken area of events bounded by green lines in the profile that seemingly traversed through the entire profile; however, the events on both sides were neat and not staggered, thus ruling out the reflection caused by the fault; the downwards sunken events were likely caused by a reduced acoustic wave velocity because of shallow gas. The reflective wave energy at the top was stable and had continuous events; the reflective wave energy at the bottom was weak and had discontinuous events and unstable waveforms. Within this area, it extended upwards in a column shape, with a width of approximately 40 m and a distance of approximately 15 m from the top to the seabed.

Characteristics of phases

The instantaneous phases of the amplitude profiles in Figs. 6 and 7 were calculated, and the instantaneous phase profiles are shown in Figs. 8 and 9, respectively. Figure 8 shows that there was an area with a disordered

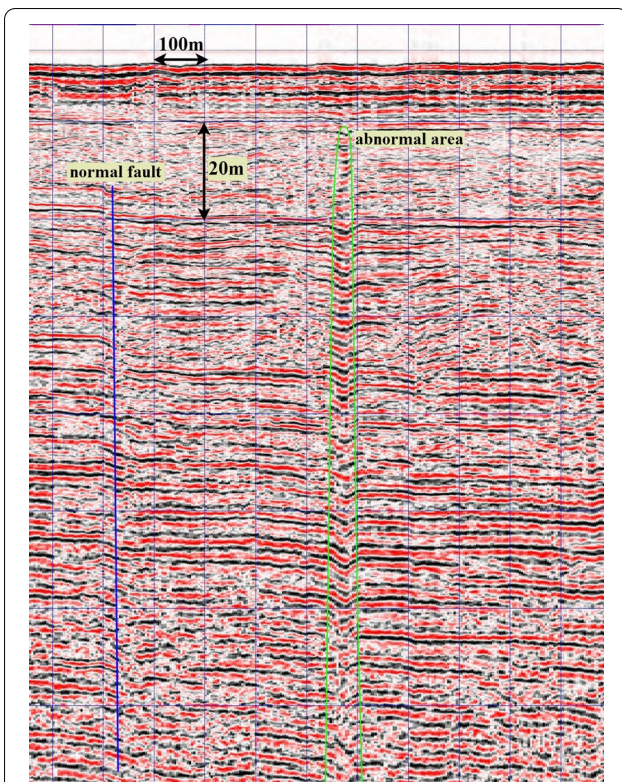


Fig. 7 Acoustic profile 2 in the survey area, and the seismic attribute is amplitude;

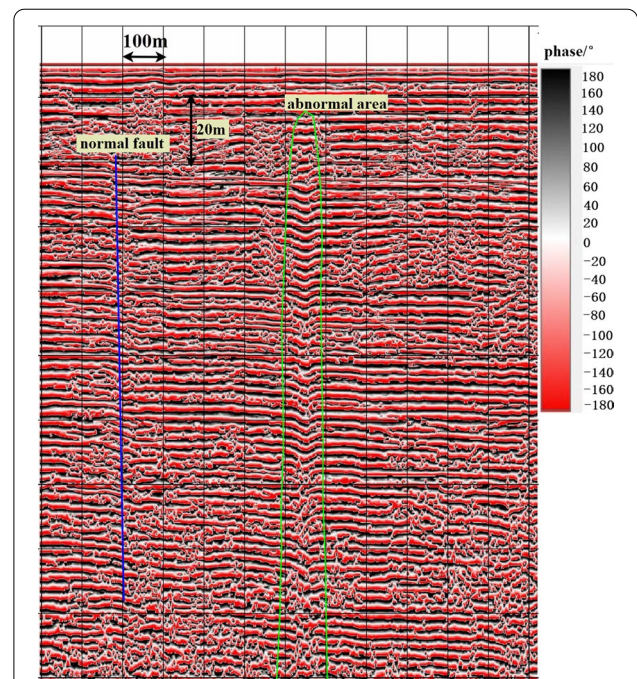


Fig. 9 Acoustic profile 2 in the survey area, and the seismic attribute is the phase for Fig. 7

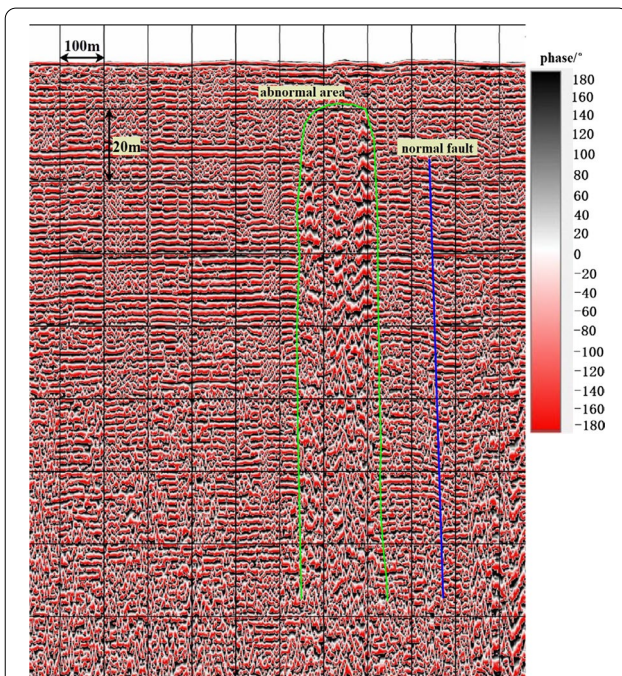


Fig. 8 Acoustic profile 1 in the survey area, and the seismic attribute is the phase for Fig. 6

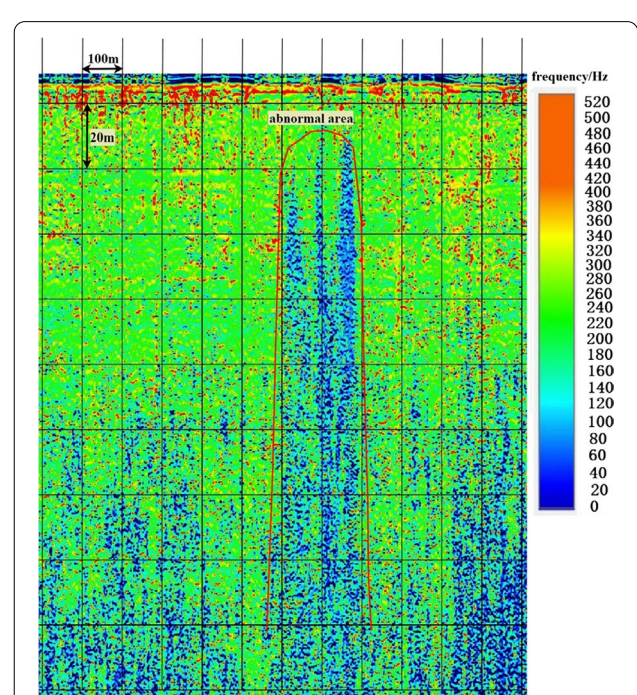
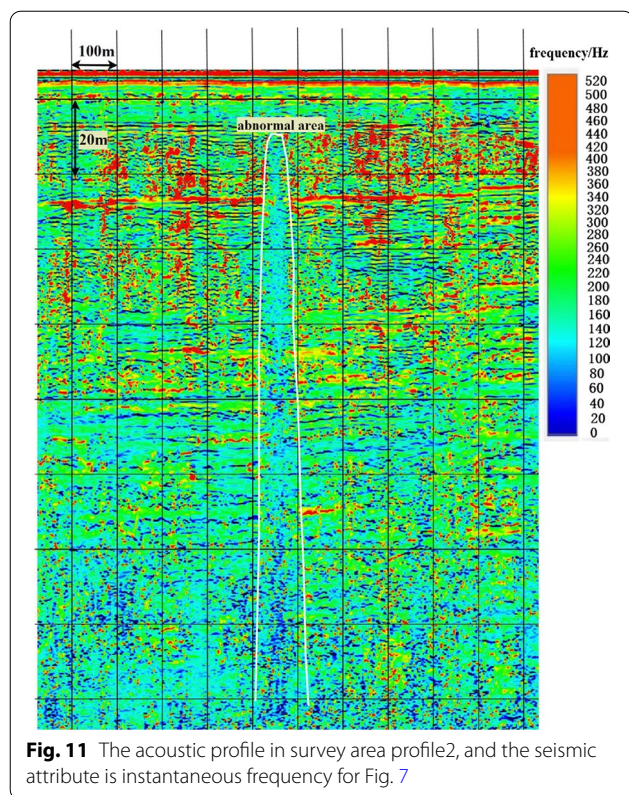


Fig. 10 The acoustic profile in survey area profile 1, and the seismic attribute is instantaneous frequency for Fig. 6



phase bounded by green lines in the middle of the profile. It was column-shaped and had a width of approximately 110 m. The distance from the top to the seabed was approximately 15 m, which was the same as the area with a disordered reflection area on the amplitude profile. In this area, there was no insignificant layered structure; furthermore, compared with events in the surrounding area, the events were significantly rougher. On its top, there was a staggered and reversed event phase.

Figure 9 shows that there was a depressed area of events bounded by green lines in the profile. It was column-shaped with a width of approximately 40 m. The distance from the top to the seabed was approximately 15 m, which was the same as the sunken event area on the amplitude profile. At the top of the area, although the events were sunken, they were still continuous; in the lower part of the area, the events gradually became noncontinuous, with a gradually unclear and disordered layered structure. On its top, there was a staggered and reversed event phase.

Characteristics of frequency

The instantaneous frequencies of the amplitude profiles in Figs. 6 and 7 were calculated, and the instantaneous frequency profiles are shown in Figs. 10 and 11, respectively. Figure 10 shows that the instantaneous frequency

of the entire profile was between 50 and 500 Hz, demonstrating a higher frequency in the upper part and a lower frequency in the lower part overall. There was an abnormal frequency area bounded by red lines in the middle of the profile. It was column-shaped and had a width of approximately 110 m. The distance from the top to the seabed was approximately 15 m, which was the same as the disordered reflection area in the amplitude profile. In this area, the high-frequency components were lost, demonstrating low-frequency characteristics. The instantaneous frequencies were 100–150 Hz, while those in the surrounding area were generally higher than 200 Hz.

Figure 11 shows that the instantaneous frequencies of the entire profile were between 50 and 500 Hz, demonstrating a higher frequency in the upper part and a lower frequency in the lower part overall. There was an abnormal frequency area bounded by white lines in the middle of the profile. It was column-shaped with a width of approximately 40 m. The distance to the seabed was approximately 15 m, which was the same as the sunken area on the amplitude profile. In this area, the high-frequency components were lost, demonstrating low-frequency characteristics. The instantaneous frequencies were 150–200 Hz, while those in the surrounding area were generally higher than 200 Hz.

Findings

Upon foregoing analysis, there were abnormal areas in the amplitude, phase and frequency profiles with approximately the same shapes and locations. According to the geological drilling data, there were mainly sand strata and a few clay strata at depths of 15–120 m beneath the seabed, which were characterized by strong permeability. However, there were mainly muddy clay strata at depths within 15 m beneath the seabed. Hence, the abnormal areas were reflections of shallow gas based on the characteristics of reflective waves, such as a weak amplitude, disordered reflection, phase reversion on the top, sunken events, and loss of high-frequency components. For the acoustic stratigraphic profiles, the spatial sampling rate $dx=2$ m; the positioning accuracy of the sound source and hydrophone was 2 m. Based on the interpretation accuracy and onsite measurement accuracy at the cross-over points, the accuracy in determining the range of shallow gas was 3 m. The distribution characteristics of shallow gas in the survey area are shown in Fig. 12.

Figure 12 shows that the shallow gas was located at the end of a normal fault whose top burial depths were 31–57 m. According to the geological drilling data, there was mainly muddy clay at a depth of 15 m below the seabed, which was an overlying well cap. Based on the seismic data of the platform site in past years, shallow gas in the strata at a depth of 60 m surrounding the platform

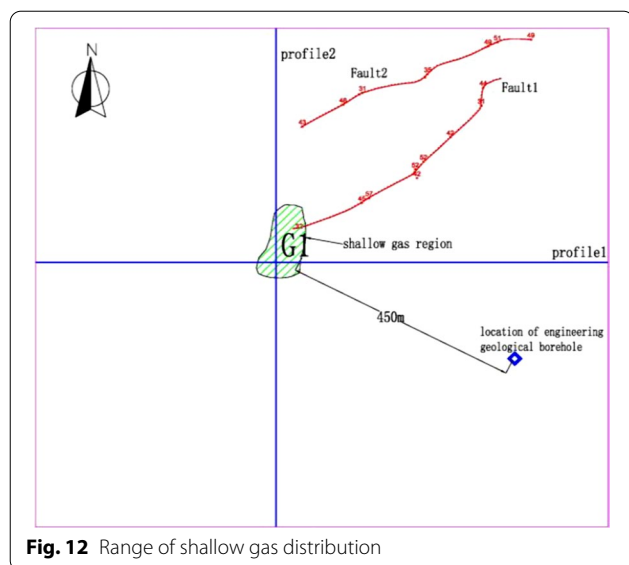


Fig. 12 Range of shallow gas distribution

appeared in the past 10 years; furthermore, the platform was located in the fault zone of Yangerzhuang-Zhaojiapu in the Chengbei fault terrace. The long-term developed Zhaobei fault and Yangerzhuang fault are not only discordogenic faults but also form oil and gas transfer passages with unconformable planes. Therefore, the faults form oil and gas reservoirs on both sides and in unconformable areas. The oil reservoir has a burial depth of 990–1985 m, a porosity of more than 30%, and a permeability of $1200\text{--}1700 \times 10^{-3} \mu\text{m}^2$.

Therefore, the abnormal areas on the profiles were reflections of shallow gas. However, a large-scale acoustic blanket requires much gas to maintain its formation (Gu et al. 2009a, b). The shallow gas was likely from the in-depth strata and transferred upwards along faults. In recent years, with increased gas pressure, the gas has transferred upwards to a location 15 m beneath the seabed by breaking the resistance of strata in column form. When muddy clay was encountered at the seabed, the gas pressure was equivalent to the resistance of the stratum, forming column-shaped shallow gas in the shallow strata.

Conclusions

Based on drilling data, a stratigraphic model of shallow gas in the seabed was established for forward simulation analysis of shallow gas in the seabed. Since the acoustic wave velocity in strata that contain shallow gas is reduced and smaller than that in the surrounding strata, the reflective wave phase at the boundary between shallow gas and strata is reversed, and there are sunken events in the interior and lower parts of the shallow gas.

An analysis of the amplitude, phase and frequency based on the acoustic stratigraphic profile of the

Huanghua Sea area in Bohai Bay revealed that there were abnormal areas in the seismic attribute profiles. Furthermore, they were of the same position and demonstrated a disordered weak amplitude reflection, top phase reversion and loss of high-frequency components. Overall, there was shallow gas reflection in the abnormal areas.

Therefore, shallow gas may be identified through the analysis of multiple seismic attributes of acoustic stratigraphic profiles, such as the amplitude, phase and frequency.

Acknowledgements

We thank Xu Hao at the CNPC Research Institute of Engineer Technology for his help in engineering geological borehole data analysis.

Author contributions

XY was responsible for most of the work of this paper, including data collection, data processing, and results analysis. MC was responsible for the field engineering geophysical survey. XL and ZY was responsible for field engineering geological drilling. All authors read and approved the final manuscript.

Funding

CNPC Scientific research and technology development project- Research on Key Technologies of offshore oil and gas pipeline design and construction (2019B-3010).

Availability of data and materials

The geological borehole data were from actual borehole sampling in Bohai Bay, which was a full coring borehole. The drilling coordinates were $38^{\circ}29'28.6651''\text{N}$, $117^{\circ}45'15.3138''\text{E}$; the water depth was 3 m, and the drilling depth was 120 m. The dates of drilling were 2020/11/14–2020/11/25. The seismic data were from the actual geophysical survey in Bohai Bay, with a survey area of $1 \text{ km} \times 1 \text{ km}$. The location of the survey was surrounded by 4 points: $38^{\circ}29'45.3961''\text{N}$, $117^{\circ}44'54.5349''\text{E}$; $38^{\circ}29'45.1273''\text{N}$, $117^{\circ}45'36.2801''\text{E}$; $38^{\circ}29'12.1228''\text{N}$, $117^{\circ}45'35.9334''\text{E}$; $38^{\circ}29'12.3916''\text{N}$, $117^{\circ}44'54.1935''\text{E}$. The survey dates were 2020/10/14–2020/10/19.

Declarations

Competing interests

The authors declare that they have no competing interests.

Author details

¹CNPC Research Institute of Engineering Technology, JinTang Road 40#, Binhai New District, Tianjin, China. ²CNPC Key Laboratory of Marine Engineering, JinTang Road 40#, Binhai New District, Tianjin, China.

Received: 15 October 2021 Accepted: 2 April 2022

Published online: 21 April 2022

References

- Gu ZF, Liu HS, Li GF et al (2009a) Genesis of shallow gas in the western area of the South Yellow Sea. *Nat Gas Ind* 29:26–29
- Gu ZF, Zhang ZX, Liu HS (2009b) Contrast between traps at the shallow sub-bottom depth and the seismic reflection features of shallow gas. *Mar Geol Quat Geol* 29:115–122
- Gu ZF, Zhang ZX, Liu HS, Lan XH (2008) Shallow geological background of shallow gas in the western south yellow sea. *Mar Sci* 32:46–51
- Guo A, Shen L, Zhang J, Qin J, Huang X, Wang Y (2010) Analysis of influence mode of shallow gas on construction of HangZhou metro. *J Railw Eng Soc* 27:78–81
- Hou YM, Li XS, Lu QG et al (2013) Research and application of spectrum attenuation attribute analysis in eliminating the influence of shallow gas. *J Pet Nat Gas* 35:96–99

- Hu GW (2010) Experimental study on acoustic responses of gas hydrates to sediments from south China sea. China University of Geosciences, Wuhan
- Lei W, Xiao HY, Deng YQ (2007) Principle of engineering and environmental geophysical exploration. Geological Publishing House, Beijing
- Li CH (2015) Seismic wave attenuation in hydrate-bearing sediments and the estimates of attenuation coefficient. China University of Geosciences, Beijing
- Li SL, Li X, Dong HP, Zhao QF (2013) Geochemistry and genetic types of hydrocarbon gases from seabed sediments in the center of South Yellow Sea. *J Oil Gas Technol* 35:20–31
- Long JJ, Li GX (2015) Theoretical relations between sound velocity and physical-mechanical properties for seabed sediments. *Acta Acoust* 40:462–468
- Mou YG, Chen XH, Li GF et al (2007) Seismic data processing method. Petroleum Industry Press, Beijing
- Orange DL, García-García A, McConnell D, Lorensen T, Fortier G, Trincardi F, Can E (2005) High-resolution surveys for geohazards and shallow gas: NW Adriatic (Italy) and Iskenderun Bay (Turkey). *Mar Geophys Res* 26:247–266. <https://doi.org/10.1007/s11001-005-3722-9>
- Sager WW, Lee CS, MacDonald IR, Schroeder WW (1999) High-frequency near-bottom acoustic reflection signatures of hydrocarbon seeps on the Northern Gulf of Mexico continental slope. *Geo-Mar Lett* 18:267–276. <https://doi.org/10.1007/s003670050079>
- Shang J, Sha Z, Liang J, Wu L (2013) Acoustic reflections of shallow gas on the Northern slope of South China sea and implications for gas hydrate exploration. *Mar Geol Front* 29:23–30
- Sun Y, Huang B (2014) A Potential Tsunami impact assessment of submarine landslide at Baiyun depression in Northern South China sea. *Geoenviron Disast* 1:7. <https://doi.org/10.1186/s40677-014-0007-0>
- Wang H-P, Zhang W, Li C-L, Wang L (2014) High resolution seismic identification of seafloor shallow geo-logical hazards. *Mar Sci* 38:103–109
- Wang K, Wang G, Cornelison B, Liu H, Bao Y (2021) Land subsidence and aquifer compaction in Montgomery county, Texas, U.S.: 2000–2020. *Geoenviron Disast* 8:1–24. <https://doi.org/10.1186/s40677-021-00199-7>
- Wang Y, Kong L-W, Guo A-G, Tian H-N (2011) Occurrence characteristics and unsaturated parameters prediction of shallow gassy sand. *Rock Soil Mech* 32:1945–1950
- Whelan T, Coleman JM, Suhayda JN, Roberts HH (1977) Acoustical penetration and shear strength in gas-charged sediment. *Mar Geotechnol* 2:147–159. <https://doi.org/10.1080/10641197709379776>
- Woodside JM, Modin DI, Ivanov MK (2003) An enigmatic strong reflector on subbottom profiler records from the black sea? The top of shallow gas hydrate deposits. *Geo-Mar Lett* 23:269–277. <https://doi.org/10.1007/s00367-003-0149-7>
- Yan ZC, Liu YP, Qu W, Qi FQ (2007) Distribution characteristics and formation causes of shallow gas in the Kuihuadao structure area of Liaodong Bay and its impact on the engineering. *Coast Eng* 26:1–10
- Yang J, Zhang BL, Zhou B (2015) Geological disaster acoustic wave identification and prediction technology of deep-water shallow gas. *Oil Drill Prod Technol* 37:143–146
- Yang XD, Ma RM, Luo XQ et al (2020) The research of detecting and identifying method for seabed shallow gas. *Coast Eng* 39:187–195
- Zou D-P, Wu B-H, Lu B, Zhang W-F, Chen F-Y (2008) Studies on clustering analysis of acoustic and physical-mechanical properties of seabed sediments. *J Trop Oceanogr* 27:12–17
- Zou DP, Wu BH, Lu B (2007) Analysis and study on the sound velocity empirical equations of seafloor sediments. *Acta Oceanogr* 29:43–50

Publisher's Note

Springer Nature remains neutral with regard to jurisdictional claims in published maps and institutional affiliations.

Submit your manuscript to a SpringerOpen[®] journal and benefit from:

- Convenient online submission
- Rigorous peer review
- Open access: articles freely available online
- High visibility within the field
- Retaining the copyright to your article

Submit your next manuscript at ► [springeropen.com](https://www.springeropen.com)
